



**CHALMERS**  
UNIVERSITY OF TECHNOLOGY

---

# **Development of a Mathematical Model for the Cooling of an Electric Car Battery**

Master's thesis in Innovative and Sustainable Chemical Engineering

VICTOR NILSSON



# Development of a Mathematical Model for the Cooling of an Electric Car Battery

VICTOR NILSSON



**CHALMERS**  
UNIVERSITY OF TECHNOLOGY

Department of Chemistry and Chemical Engineering  
*Division of Chemical Engineering*  
CHALMERS UNIVERSITY OF TECHNOLOGY  
Gothenburg, Sweden 2017

Development of a Mathematical Model for the Cooling of an Electric Car Battery  
VICTOR NILSSON

© VICTOR NILSSON, 2017.

Supervisor: Dr. Fredrik Jareman, ÅF

Examiner: Associate Professor Ronnie Andersson, Department of Chemistry and  
Chemical Engineering

Department of Chemistry and Chemical Engineering

Division of Chemical Engineering

Chalmers University of Technology

SE-412 96 Gothenburg

Telephone +46 31 772 1000

Typeset in L<sup>A</sup>T<sub>E</sub>X

Gothenburg, Sweden 2017

## Abstract

Electric car batteries deal with problems not present in traditional cars propelled by combustion. Since the battery is the sole power source, large amount of heat is produced which can lead to overheating. This is mitigated with thermal management systems and there exists different possible technological solutions. The objective of this study was to develop a mathematical model in GT-Suite for predicting and investigating the thermal behaviour of an electric car battery in response to coolant flow rate and design choices. The model was limited to only one battery module (a group of cells) and only the cooling of battery cells was studied.

The model was able to complete simulations of fully depleting the battery at steady power requests under one minute and was independent of spatial resolution. Too large time step lead to instabilities in the coolant pump. The assumptions of a uniform pipe wall surface temperature and neglectable internal heat resistance of the battery cells were deemed acceptable. The largest thermal resistance was present in the space between the coolant pipe and the battery cells. The results were very sensitive to the specified properties of this space. Using real data, it is crucial that these parameters are correctly set. In reality, the large heat transfer resistance between the pipe and the battery cells is probably decreased by filling the space with something other than air, but due to lack of data this could not be confirmed.

The flow inside the coolant pipe was laminar in all the simulations. It was deemed unfeasible to increase the flow rate to such a level that turbulence was created. To increase the convective heat transfer inside the coolant pipe, turbulence could be induced by adding dimples. This could not be implemented in the software without adding new correlations to the code, which was not done due to time limitations.

The model was assumed to be suitable for conceptual studies and early-stage modelling after further developments have been implemented, most importantly adding electrical circuits and expanding the model to include a whole battery pack with correct boundary conditions. In addition, real battery data is needed to validate the model before any real conclusions can be drawn about its validity.

Keywords: EV, BTM, BTMS, electric, car, battery, model, thermal, management.



## Acknowledgements

I would like to thank Dr. Fredrik Jareman for his supervision and Christoffer Källerman for his technical support, and all the others at ÅF who have helped me.

The support from Gamma Technologies has been greatly appreciated. Both because of the academic license and for their great technical support, in particular that from Nikolaos Papadopoulos, Peter Stopp, and Joe Wimmer.

I would also like to thank my examiner Associate Professor Ronnie Andersson at Chalmers University of Technology for his support and advice.

Victor Nilsson, Gothenburg, June 2017



# Nomeclature

## Quantities

### *Latin Letters*

$A$	area [m <sup>2</sup> ]
$A_{cs}$	cross-sectional area [m <sup>2</sup> ]
$A_{floor}$	area of portion of module floor [m <sup>2</sup> ]
$A_{roof}$	area of portion of module roof [m <sup>2</sup> ]
$A_s$	heat transfer surface area [m <sup>2</sup> ]
$a$	height of the pipe minus $b$ [m]
$b$	width of the pipe [m]
$C$	Coloumbic efficiency
$C_f$	Fanning friction factor
$C_{f,rough}$	Fanning friction factor of a rough pipe
$C_{max}$	maximum Courant number
$C_p$	specific heat capacity [J/(kg · K)]
$C_t(T)$	the temperature coefficient [V/K]
$D$	pipe diameter or hydraulic pipe diameter [m]
$D_H$	hydraulic pipe diameter [m]
$dp$	pressure difference across $dx$ [Pa]
$dx$	discretization length [m]
$E\text{-rate}$	rate at which power is supplied from battery
$H$	total specific enthalpy [J/kg]
$h$	convective heat transfer coefficient [W/(m <sup>2</sup> · K)]
$h_{ex}$	exterior convective heat transfer coefficient of module wall [W/(m <sup>2</sup> · K)]
$h_{g,rough}$	convective heat transfer coefficient at a rough pipe [W/(m <sup>2</sup> · K)]
$h_i$	convective heat transfer coefficient of the coolant pipe [W/(m <sup>2</sup> · K)]
$I$	electrical current [A]
$K_f$	friction losses coefficient
$K_p$	pressure loss coefficient
$k$	slope
$L$	length of pipe object [m]
$L_b$	length of solid body [m]
$l$	width of air-gap [m]
$\dot{m}$	mass flow [kg/s]
$Nu$	Nusselt number
$P$	pressure [Pa]
$P_J$	(irreversible) Joule heating [W]
$P_{REQUEST}$	power request from lumped battery cells [W]
$Pr$	Prandtl number
$q_{cd}$	conductive heat flux [W/m <sup>2</sup> ]
$q_{cv}$	convective heat flux [W/m <sup>2</sup> ]

---

$q_{irrev}$	(irreversible) Joule heating [W/m <sup>2</sup> ]
$R$	electrical resistance [ $\Omega$ ]
$R_b$	radius of the bend (from the center of the bend to the center of the pipe) [m]
$R_{int}$	internal resistance of battery cells [ $\Omega$ ]
$R_T$	thermal resistance [K/W]
$Re_D$	Reynolds number
$r$	thickness of pipe wall and battery module wall [m]
$SOC$	state of charge
$\nabla T$	temperature gradient [K/m]
$T$	the cell temperature [K]
$T_{fluid}$	fluid temperature [K]
$T_{wall}$	wall temperature [K]
$T_i$	initial temperature [K]
$\Delta t$	time step [s]
$t$	time [s]
$u$	fluid flow speed [m/s]
$\Delta V$	voltage [V]
$V$	volume [m <sup>3</sup> ]
$V_C$	delivered voltage [V]
$V_{OC}$	open circuit voltage [V]
$\Delta x$	cell size [m]
$x$	input
$y(t)$	output
$y_{initial}$	initial output

*Greek Letters :*

$\varepsilon$	pipe wall sand roughness height [m]
$\theta$	angle of pipe bend [ $^\circ$ ]
$\lambda$	thermal conductivity [W/(m · K)]
$\mu$	dynamic viscosity [Pa·s]
$\nu$	kinematic viscosity [m <sup>2</sup> /s]
$\rho$	density [kg/m <sup>3</sup> ]

<b>Modelling Objects</b>	<b>Used in GT-Suite</b> (see section 3)
<i>Battery</i>	Models lumped battery cells
<i>ConductionConn</i>	Models heat conduction
<i>ConvectionConn</i>	Models heat convection
<i>EndEnvironment</i>	Sets boundary conditions for inlet and outlet flow
<i>PIDController</i>	Models the PID-Controller
<i>PipeCrossSection</i>	Models the pipe flow
<i>Pump</i>	Models the pump
<i>PumpSpeed</i>	Sets the speed of the pump
<i>Temperature</i>	Sets temperature as boundary condition
<i>ThermalBlock</i>	Models solid three-dimensional parts
<i>ThermalMass</i>	Models solid one-dimensional parts

# Contents

<b>1</b>	<b>Introduction</b>	<b>1</b>
1.1	Background . . . . .	1
1.2	Objectives . . . . .	2
1.3	Limitations . . . . .	2
<b>2</b>	<b>Theory</b>	<b>5</b>
2.1	Electrochemistry of Battery . . . . .	5
2.2	Electric Circuits . . . . .	5
2.3	Battery Physics and Modelling . . . . .	6
2.4	Thermal Management of Car Battery and Its Structure . . . . .	7
2.5	Discretization and Solving the Governing Equations . . . . .	7
2.5.1	Implicit Time Step Method . . . . .	7
2.6	Mass Transport . . . . .	8
2.7	Momentum Transport . . . . .	8
2.7.1	Friction Losses . . . . .	8
2.7.2	Total Pipe Bend Losses . . . . .	9
2.8	Heat Transport . . . . .	9
2.8.1	Modelling Wall Temperature . . . . .	10
2.8.2	Thermal Conduction . . . . .	10
2.8.3	Thermal Convection at the Wall . . . . .	10
2.8.4	Quantities for Investigating Sensitivity and Assumptions . . . . .	11
2.9	Control Theory . . . . .	12
2.9.1	Step Response . . . . .	12
<b>3</b>	<b>Model</b>	<b>13</b>
3.1	Overview of System . . . . .	13
3.2	Parameters . . . . .	13
3.3	Model Formulation in GT-Suite . . . . .	14
3.3.1	Heat Convection ( <i>ConvectionConn</i> ) . . . . .	14
3.3.2	Heat Conduction ( <i>ConductanceConn</i> ) . . . . .	14
3.3.3	Pump ( <i>Pump</i> and <i>PumpSpeed</i> ) . . . . .	15
3.3.4	Pipe ( <i>PipeCrossSection</i> ) . . . . .	15
3.3.5	Flow Boundary ( <i>EndEnvironment</i> ) . . . . .	15
3.3.6	Solid Walls ( <i>ThermalMass</i> ) . . . . .	16
3.3.7	Battery Cells ( <i>ThermalBlock</i> ) . . . . .	16
3.3.8	Battery Cells ( <i>Battery</i> ) . . . . .	17

3.3.9	Controller ( <i>PIDController</i> ) . . . . .	18
3.3.9.1	Tuning the Controller . . . . .	18
3.3.10	Temperature ( <i>Temperature</i> ) . . . . .	18
3.4	Modelling the Coolant Circuit . . . . .	18
3.5	Modelling Heat Transfer . . . . .	19
3.5.1	Pipe to Battery Cells . . . . .	19
3.5.2	Pipe to Outside Module . . . . .	19
3.5.3	Battery Cells to Outisde Module . . . . .	20
3.5.4	Battery Cells to Battery Cells . . . . .	20
<b>4</b>	<b>Results and Discussion</b>	<b>21</b>
4.1	Heat Production . . . . .	21
4.2	Cell Temperature . . . . .	22
4.3	Heat Transfer . . . . .	27
4.3.1	Assumptions . . . . .	27
4.3.2	Sensitivity Analysis and Heat Transfer Optimization . . . . .	28
4.4	Controller . . . . .	30
4.5	System Data . . . . .	30
<b>5</b>	<b>Conclusions and Future Work</b>	<b>31</b>
	<b>Bibliography</b>	<b>33</b>
<b>A</b>	<b>Appendix</b>	<b>I</b>

# 1

## Introduction

### 1.1 Background

The interest in and development of electric cars has increased continuously since the year 2000. Apart from the advantage of no emissions while driving, the efficiency of an electric car motor is above 90 % compared to a combustion engine of 37 %. It would be misleading though not to mention that the power source of an electric car, i.e. the battery, comes with its own energy losses and maintenance issues which need to be improved [1].

There exist several types of electric vehicle batteries (EVB), all with the required properties such as being able to supply power over sustained periods of time and to be recharged. Some examples of EVB technologies include lithium-ion, nickel cadmium, and nickel metal hydride batteries [1]. Compared to other types of batteries, EVB have a high power-to-weight ratio but still have much lower specific energy compared to liquid fuels [2, 3, 4].

The energy density of lithium-ion batteries commonly used in electrical vehicles (EV) and hybrid electrical vehicles (HEV) have increased over the last decades [3, 4]. This requires efficient thermal management of the battery since heat is generated in the battery cells and its electrical circuits both during charge and discharge [5, 6]. Fig. 1.1 shows a simplified structure of the battery (i.e. battery pack) and its internal components. It is crucial that these cells are not overheated since this will increase the energy consumption and shorten their lifetime [7]. Elevated temperatures increase the rate of the electrochemical reactions which tends to increase the performance of the battery, but this comes with the cost of increased corrosion leading to a shorter battery lifetime. The battery's working-temperature should preferably be in the span of 20 °C and 40 °C, since a too low temperature limits the amount of power the battery can deliver [8]. To avoid short circuits, the temperature difference between the cells should not exceed 5 °C [9]. This can be handled with internal cooling of the battery, e.g. by pumping a coolant through it [10].

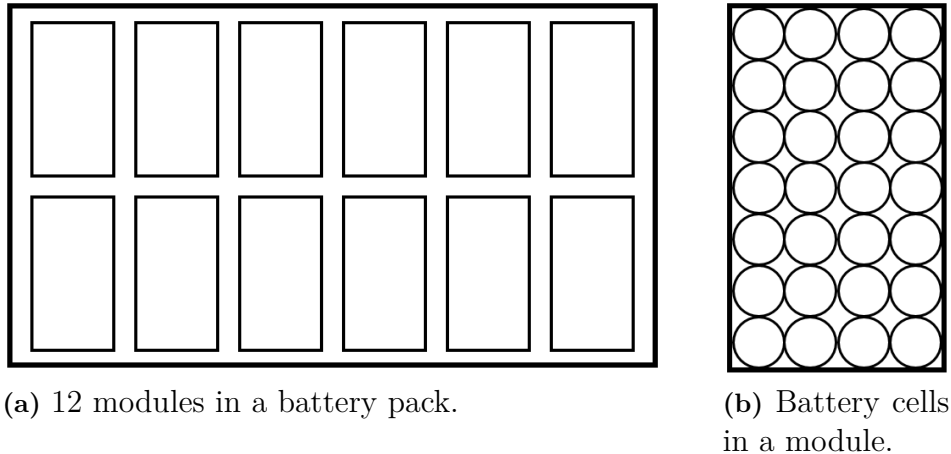


**Figure 1.1:** Simplified overview of a battery pack

Extensive studies have been performed on modelling battery cells through-out their charge-discharge cycles, like their resistance, state of charge, heat generation, temperature, etc [7]. This can be done on several levels; on an electrochemical level [11, 12], by modelling the cells as electric circuits [13], or by a combination of these two modelling approaches [14].

Studies have been conducted on the modelling of the thermal management of the batteries. This includes not just the cooling but also the heating of battery cells [8]. The majority of the studies focusing on the cooling of batteries have only studied the exterior cooling of the battery, disregarding the interior thermal management. When studying the internal heat transport, the aim has not been to produce models that can perform rapid simulations. Instead a more detailed level of modelling has been favoured with the cost of longer simulation time [15, 16].

## 1.2 Objectives

The objective of this project is to develop a transient 1D model based on Tesla Model S in the commercial software GT-Suite to predict the temperature of the battery cells for different power requests. The model will be used to investigate how the temperature of the battery and its cells can be controlled with the coolant pump flow speed. Further, it will be investigated how the internal and external heat transfer can be manipulated by design choices. The effects of spatial and temporal resolution on the results will be investigated.

## 1.3 Limitations

The system will be limited to model a part of the battery known as a module, which are combined together to form the battery pack. The exterior convective heat transfer coefficient of the wall of the battery module is not modelled but defined according to Table 3.1. The conductive thermal resistance in air-gaps is also constant

by specified size and thermal conductivity. The heat transfer inside the battery cells is not resolved, and cells are lumped into groups. The power supplied from the battery is specified (see section 4) and constant throughout each simulation. In some simulations the battery efficiency is defined to increase the heat production (see section 4). Active heating of the battery cells is not investigated.



# 2

## Theory

### 2.1 Electrochemistry of Battery

There exists a variety of types of batteries which relies on different chemistry in the cells. As of writing, the most common type of battery in electric cars is Lithium-ion batteries. In the cell, two electrodes are present which are in contact with electrolyte. A redox-reaction takes place in the cell with the electrolyte acting as a medium for lithium ions to move while electrons move through an external closed circuit between the electrodes. During discharge, the lithium-ions and electrons move towards the positive electrode (cathode) composed of a lithium compound. When the electrons move through the external circuit in this manner, useful work can be performed when connected to a device which the electrons moves through. During charging of the cell, the reverse process is taking place [17, 18].

### 2.2 Electric Circuits

Ohm's law specifies

$$\Delta V = IR, \quad (2.1)$$

where  $\Delta V$  is the voltage over the unit [V],  $I$  is the current [A], and  $R$  is the resistance [ $\Omega$ ]. For a series of units, the current is constant through each unit, and calculating the resistance over a series of units is calculated as

$$R_{series} = \sum_{i=1}^{units} R_i, \quad (2.2)$$

which can be used to calculate the potential over the series of units. For parallel units, the voltage is equal over each unit and the total resistance over the units is calculated as

$$\frac{1}{R_{parallel}} = \sum_{i=1}^{units} \frac{1}{R_i}, \quad (2.3)$$

The phenomena known as Joule heating in its most general form is

$$P_J = \Delta V \cdot I, \quad (2.4)$$

where  $P_J$  is the power of generated thermal energy in the unit [W] [6].

## 2.3 Battery Physics and Modelling

State of Charge (SOC) of the battery is defined as

$$SOC = \frac{\text{Instantaneous Capacity}}{\text{Maximum Capacity}}, \quad (2.5)$$

where the maximum capacity [A·h], and instantaneous capacity [A·h]. The former is a given quantity and the latter is modelled as

$$\text{Instantaneous Capacity} = \text{Initial (Instantaneous) Capacity} - \int_t I dt, \quad (2.6)$$

where the *Initial (Instantaneous) Capacity* is specified, and the current  $I$  is calculated as

$$I = \frac{V_{OC} - \sqrt{V_{OC}^2 - 4R_{int} \cdot P_{REQUEST} \cdot C}}{2R_{int}}, \quad (2.7)$$

where  $R_{int}$  is the internal resistance [ $\Omega$ ], and  $V_{OC}$  open circuit voltage [V], and both are defined as functions of SOC and temperature [K]. They are defined by data points which the functions are fit to.  $C$  is the coulombic efficiency which describes how efficient the electrons in the system are transferred (specified in this study as unity due to limited access to data), and  $P_{REQUEST}$  is the power requested from the battery cells [W]. Imaginary roots are possible for eq. (2.7) as a result of a higher power supply than possible. In this case the maximum possible current is used [19].

The E-rate is a term describing the discharge power (i.e. the power request) relative to the battery capacity [20]. An E-rate of 1E means that the battery will be discharged in 1 hours, 2E means 0.5 hours, E/2 means 2 hours, and so on.

The instantaneous heat released (dissipated) in the battery is given as

$$q = I \cdot (V_{OC} - V_C) - I \cdot T \cdot C_t(T), \quad (2.8)$$

where  $V_C$  is the delivered voltage [V],  $T$  is the battery temperature [K], and  $C_t(T) = (dV_{OC}/dT)$  is the temperature coefficient [V/K] [5, 19]. The two terms on the right-hand side in eq. (2.8) are due to irreversible Joule heating ( $I \cdot (V_{OC} - V_C)$ ) and reversible entropic heat ( $I \cdot T \cdot C_t(T)$ ). The former is due to the internal resistance of the cell and the latter to isentropic changes from the electrochemical reactions. The one due to the internal resistance can be expressed as

$$q_{irrev} = R \cdot I^2, \quad (2.9)$$

to show that the first term always is positive. The second term on the right-hand side in eq. (2.8) can be positive or negative, but the first term dominates the model leading to a heat being released both during discharging and charging of the battery. The delivered voltage is calculated as

$$V_C = V_{OC} - IR_{int}. \quad (2.10)$$

## 2.4 Thermal Management of Car Battery and Its Structure

The units that generate the electrical energy in the battery pack (i.e. the battery) are the battery cells. These are grouped together for easier handling during manufacturing, and these units are called modules. The cells in the module can be connected in series, parallel, or both. The modules are in turn grouped together to form the battery pack, see Fig. 1.1 for an overview [21]. There are a number of different battery thermal management systems (BTMSs); air cooling versus liquid cooling, and passive versus active cooling [10].

For instance, the Tesla S the battery pack consists of 16 modules located beneath the seats and are cooled with coolant pumped through one loop for each module [22, 23, 24]. In this case, two systems are present: passive air cooling acting on the battery pack walls, and active liquid cooling acting inside the battery. The former is taking place simply by air flowing under the car adjacent to the battery; the latter by the flow of liquid through the internal system of the battery pack, which in turn can be designed in varying ways.

## 2.5 Discretization and Solving the Governing Equations

The governing equations that are solved for the flow and temperature are the continuity equation, the momentum equation (i.e. the Navier-Stokes equation), and the energy equation. The primary solution variables are mass flow, pressure, and total enthalpy. They are all solved in 1D.

The whole system is divided up into many discrete volumes (i.e. spatial discretization) called cells. The scalar entities of the system (e.g. pressure, temperature, etc.) are uniform over each cell, and the vector entities (e.g. velocity) are uniform over each cell boundary. This approach is called "staggered grid" [19].

### 2.5.1 Implicit Time Step Method

The two basic approaches for solving the time dependent equations are the explicit and the implicit methods. In the explicit solver, old values are used to calculate new values. In the implicit solver, old values and new values are used to calculate the new values; this solver uses iterative calculations. They both have their advantages: the explicit solver is fast on a per time step basis while the implicit solver is robust and can take larger time steps [25]. In this study, the implicit solver is used and the time step is fixed (i.e. non-dynamic). From previous experience with similar systems, the time step was initially specified to 500 ms. This was validated by confirming that

the CFL-condition was satisfied. In 1D, this condition is expressed as

$$\frac{u\Delta t}{\Delta x} \leq C_{max}, \quad (2.11)$$

where  $u$  is the speed of the flow [m/s],  $\Delta t$  is the time step [s],  $\Delta x$  is the cell size [m], and  $C_{max}$  is the largest allowed Courant number. The maximum Courant number is usually unity when an explicit method is used, but larger values can be specified when an implicit method is used [26].

## 2.6 Mass Transport

The transport of mass is governed by continuity;

$$\frac{dm}{dt} = \sum_{boundaries} \dot{m}, \quad (2.12)$$

where  $m$  is mass [kg],  $\dot{m}$  is the boundary mass flow into the volume [kg/s] ( $= [\rho Au]$ ),  $\rho$  is the fluid density [kg/m<sup>3</sup>],  $A$  is the cross-sectional flow area [m<sup>2</sup>],  $u$  is the fluid velocity [m/s].

## 2.7 Momentum Transport

The transport of momentum is described by

$$\frac{d\dot{m}}{dt} = \frac{dp \cdot A + \sum_{boundaries} (\dot{m}u) - 4C_f \frac{\rho u |u| dx \cdot A}{2D} - K_p \left( \frac{1}{2} \rho u |u| \right) A}{dx}, \quad (2.13)$$

where  $dx$  is the discretization length [m],  $dp$  is the pressure difference across  $dx$  [Pa],  $C_f$  is the Fanning friction factor,  $D$  is the pipe diameter or hydraulic diameter [m], and  $K_p$  is the pressure loss coefficient (due to e.g. bend, taper, or restriction).

### 2.7.1 Friction Losses

The friction factor  $C_f$  in eq. (2.13) in pipes is calculated by an explicit approximation of the Colebrook function where  $C_f$  is a function of Reynolds number and wall roughness. The approximation depends on the flow regime.

In the laminar flow regime ( $Re_D < 2000$ ) the friction factor is calculated as

$$C_f = \frac{16}{Re_D}, \quad (2.14)$$

where  $Re_D$  is the Reynolds number defined as

$$Re_D = \frac{uD}{\nu}, \quad (2.15)$$

where  $\nu$  is the kinematic viscosity [m<sup>2</sup>/s].

For smooth pipes with flows in the fully turbulent regime ( $Re_D > 4000$ ),  $C_f$  is calculated as

$$C_f = \frac{0.08}{Re_D^{0.25}}. \quad (2.16)$$

For pipes with rough walls, the value of the friction factor is selected as the larger of eq. (2.16) and that given by the Nikuradse formula;

$$C_{f,rough} = \frac{0.25}{\left(2 \cdot \log_{10}\left(\frac{D}{2\varepsilon}\right) + 1.74\right)^2}, \quad (2.17)$$

where  $\varepsilon$  is the pipe wall sand roughness height.

In the transition regime ( $2000 < Re_D < 4000$ ),  $C_f$  is calculated by linear interpolation between the laminar value of eq.(2.14) and the turbulent value of eq.(2.16) or (2.17), for the current  $Re_D$ .

### 2.7.2 Total Pipe Bend Losses

To calculate the total pipe bend loss, which is the sum of the pipe bend loss and friction loss. In this study the friction losses coefficient (originally included in eq. (2.13) as  $4C_f dx/D$ ) is calculated as

$$K_f = 4C_f \frac{L}{D} = 4C_f \theta \frac{\pi R_b}{180 D}, \quad (2.18)$$

where  $\theta$  is the angle of the pipe bend [°],  $R_b$  is the radius of the bend (from the center of the bend to the center of the pipe) [m], and  $L$  is the length of the pipe bend [m].

The pipe bend losses included by the pressure loss coefficient is calculated as

$$K_P = 0.25 \cdot \beta(1 + \beta/2) \cdot \phi(1.2 - 0.4\phi + 1.2[1 - \phi/2]^3), \quad (2.19)$$

$$\beta = \min\left(\frac{D}{R_b}, 2.5\right) \quad \text{and} \quad \phi = \min\left(\frac{\theta}{90}, 1.999\right). \quad (2.20)$$

$K_p$  and  $K_f$  are summed up and converted to a pressure drop by

$$\Delta P = (K_p + K_f) \frac{\rho u |u|}{2}. \quad (2.21)$$

## 2.8 Heat Transport

The transport of heat is governed by total enthalpy, and they both neglect radiation and pure conduction. The equation for total enthalpy is

$$\frac{d(\rho HV)}{dt} = \sum_{boundaries} (\dot{m}H) + V \frac{dp}{dt} - hA_s(T_{fluid} - T_{wall}), \quad (2.22)$$

where  $H$  is the total specific enthalpy [J/kg],  $h$  is the heat transfer coefficient for convection [W/(m<sup>2</sup>·K)],  $A_s$  is heat transfer surface of the wall [m<sup>2</sup>],  $T_{fluid}$  is the fluid temperature [K], and  $T_{wall}$  is the wall temperature [K].

### 2.8.1 Modelling Wall Temperature

There exists several ways of modelling the wall temperature (i.e. the temperature of the pipe or the module wall). In this project, the wall temperature is set equal to the connected *ThermalMass*-object. For more details on the *ThermalMass*-object, see section 3.3.6

### 2.8.2 Thermal Conduction

Conduction is modelled using Fourier's law:

$$q_{cd} = -\lambda \nabla T, \quad (2.23)$$

where  $q_{cd}$  is the conductive heat flux [W/m<sup>2</sup>],  $\lambda$  is the material's thermal conductivity [W/(m·K)], and  $\nabla T$  is the temperature gradient [K/m]. Conduction is for example taking place inside the solid objects, the space between the pipe and the battery cells, and the space between the lumped battery cells.

### 2.8.3 Thermal Convection at the Wall

The thermal convection at walls (e.g. pipe walls and module walls) is modelled as

$$q_{cv} = h(T_{fluid} - T_{wall}), \quad (2.24)$$

where  $q_{cv}$  is the convective heat flux [W/m<sup>2</sup>]. The convective heat transfer coefficient can either be specified or modelled. For laminar flows, meaning  $Re_D \leq 2000$ ,  $h$  is calculated as

$$h = \frac{Nu \cdot \lambda}{D}, \quad (2.25)$$

where  $Nu$  is the Nusselt number and equal to 3.66 in this study. The assumption of a constant  $Nu$  at 3.66 is based on two simplification: first, it is assumed that there is no or negligibly small axial heat conduction, which is valid for an uniform temperature across the surface [27]. The second simplification is that  $Nu$  for the pipe is assumed to be approximately the same as for a circular pipe, instead of e.g. a rectangular one (see Fig. 3.1b for the geometry of the coolant pipe) [28]. The former assumption will have to be validated after the simulation. Notice that the roughness of the pipe does not effect the heat transfer when the flow is laminar.

In a turbulent flow, the heat transfer coefficient of convection inside of a smooth pipe to the wall is calculated using the Colburn analogy:

$$h = \frac{1}{2} C_f \rho u C_p Pr^{-2/3}, \quad (2.26)$$

where  $u$  is the effective velocity outside the boundary layer [m/s],  $C_p$  is the specific heat capacity [J/(kg · K)], and  $Pr$  is the Prandtl number and defined as

$$Pr = \frac{C_p \mu}{\lambda}, \quad (2.27)$$

where  $\mu$  is the dynamic viscosity [Pa·s].

$h$  for rough pipes,  $h_{g,rough}$ , is calculated using

$$h_{g,rough} = h \left( \frac{C_{f,rough}}{C_f} \right)^n, \quad (2.28)$$

$$n = 0.68 Pr^{0.215}, \quad (2.29)$$

where  $C_{f,rough}$  is the Fanning friction factor of a rough pipe. When

$$\frac{C_{f,rough}}{C_f} > 4,$$

the heat transfer coefficient no longer increases with increasing roughness.

#### 2.8.4 Quantities for Investigating Sensitivity and Assumptions

To evaluate an area's ability to resist the flow of heat, a thermal resistance can be calculated. A high value implies high resistance to heat flow, and vice versa. It is the inverse of thermal conductance. For conduction, thermal resistance is calculated as

$$R_T = \frac{L}{\lambda A}, \quad (2.30)$$

where  $R_T$  is the thermal resistance [K/W]. For convection it is calculated as

$$R_T = \frac{1}{hA}. \quad (2.31)$$

The Biot number,  $Bi$ , is defined as the ratio of the heat transfer resistance inside a solid body and the resistance at the surface of the solid body. It is calculated as

$$Bi = \frac{L_b h}{\lambda}, \quad (2.32)$$

where  $L_b$  is the length of the body [m],  $h$  is the heat transfer coefficient at the surface of the body, and  $\lambda$  is the conductance inside the body. Usually the assumption of negligible internal resistance in a system is made when  $Bi$  is below 0.1 [29].

## 2.9 Control Theory

### 2.9.1 Step Response

A system can be modelled as

$$y(t) = y_{initial} + k \cdot \Delta x(1 - e^{-t/\tau}), \quad (2.33)$$

where  $t$  is time,  $x$  is the input to the system,  $y$  is the output of the system,  $y_{initial}$  is the initial output of the system,  $k$  is the slope, and  $\tau$  is the time constant [30].

A step response of a system is produced by abruptly (ideally over an infinitesimal time) changing the input when system is at steady-state, and consists of the output time-evolution. Information can be extracted from this process and used to tune the controllers for the system. These parameters are *settling time*, *time constant*, and *slope*.

The *settling time* is defined as the time needed for the output to reach and stay inside a specified percentage of the final output. In this study, it is set to 90.84% of the final output.

The *time constant*  $\tau$  is defined as the time needed for the output to reach 63.2% of the difference between the final and initial. That is,

$$y(\tau) = y_{initial} + k \cdot \Delta x(1 - e^{-1}) = y_{initial} + \Delta y \cdot 0.632. \quad (2.34)$$

The *slope* is defined as

$$k = \frac{\Delta y}{\Delta x} = \frac{y_{final} - y_{initial}}{x_{final} - x_{initial}}. \quad (2.35)$$

# 3

## Model

### 3.1 Overview of System

The battery system of the Tesla Model S with a 85 kWh battery described in section 2.4 is used as a base for the developed battery module model. It is cooled by a coolant that flows through tubes inside the battery module and around the rows of battery cells (see Fig. 3.1a) [31, 32]. In this model the cells are lumped into groups of three per row of cells, to a total of 21 groups of lumped cells per module. The coolant flow for the whole battery pack is splitted and led into each module separately. The geometry of the coolant pipe can be seen in Fig. 3.1b.

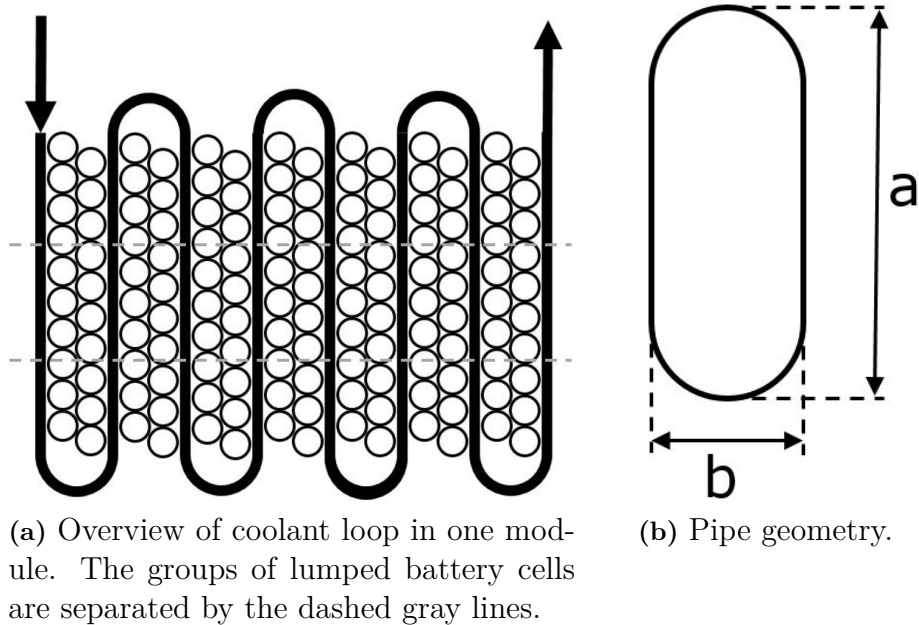


**Figure 3.1:** Geometry of the system.

### 3.2 Parameters

In this project, the heat transfer medium (coolant) is a 50 vol% water/glycerol mixture that will be flowing through coolant pipe inside the modelled battery module

which is placed surrounding the groups of cells. All solid materials are specified as aluminum. The physical data is available in GT-Suite [33, 34].

The specified parameters are pressure,  $P$ ; initial temperature of the system (including coolant inlet temperature and ambient temperature),  $T_i$ ; width of air-gaps (present e.g. between pipe wall and lumped battery cells, between pipe wall and module wall, between lumped battery cells, etc.),  $l$ ; dimensions of the pipe,  $a$  and  $b$  (see Fig. 3.1b); length of each pipe object,  $L$ ; exterior convective heat transfer coefficient of the battery module wall,  $h_{ex}$ ; thickness of solid parts (pipe wall and module wall),  $r$ ; and mass of lumped battery cells,  $m_c$  [35].

**Table 3.1:** The set parameters of the model, all arbitrarily selected (all in SI units unless otherwise specified).

$a$	$b$	$L$	$l$ [mm]	$r$ [mm]	$m_c$	$T_i$ [°C]	$P$ [bar]	$h_{ex}$
0.1	0.02	0.186	1.6	4	1	25	1	5

### 3.3 Model Formulation in GT-Suite

In GT-Suite, the different parts and phenomena of the system (e.g. pipe walls, pump, battery cells, battery module walls, heat conduction, fluid flow, boundaries, etc.) are represented and modelled by different so called *objects*. Information is transferred between them (e.g. heat and flow) by using *connectors*. The *objects* are presented below based on their function with the *object's* name in parenthesis in the headline.

#### 3.3.1 Heat Convection (*ConvectionConn*)

The convection of heat is modelled using the object *ConvectionConn*. In the object, the convective heat transfer coefficient [W/m<sup>2</sup>K] is modelled with eq. (2.26), (2.25), or (2.28), and the surface area [m<sup>2</sup>] is supplied from the connected *ThermalMass*-object. *ConvectionConn* is used to model the heat transfer between the pipe and the battery cells, the pipe and the battery module walls, the battery cells and the battery module walls, the module walls and the surrounding air.

#### 3.3.2 Heat Conduction (*ConductanceConn*)

The conduction of heat is modelled using the object *ConductanceConn*. In the object, thermal conductance per unit area [W/m<sup>2</sup>K] and surface area are specified. The former is defined as thermal conductivity divided by the distance of conduction. This object models the heat transfer through stagnant air (e.g. between the lumped battery cells, between the pipe and the battery module-wall, etc.). The thermal conductance per unit area,  $\lambda/l$ , is calculated to 15 W/m<sup>2</sup>K from a given  $\lambda$  of 0.024 W/mK [29] and  $l$  arbitrarily set to 1.6 mm (the effects of this assumption is investigated in section 4). In this study, the surface area is set equal to the smallest

of the areas of the objects *ConductanceConn* is connected to. For examples of these connections, see Fig. 3.5, 3.6, and 3.7.

### 3.3.3 Pump (*Pump* and *PumpSpeed*)

The object *Pump* is used to model the Pump. For this to work, a pump performance map is supplied (already present in GT-Suite) where relations between pump speed, volumetric flow rate, pressure rise, temperature, and isentropic efficiency are defined. The object *PumpSpeed* is connected to *Pump* to control the imposed speed [RPM] and the initial angular position [°].

### 3.3.4 Pipe (*PipeCrossSection*)

The geometry of the pipe is shown in Fig. 3.1b. The cross-sectional area is calculated as

$$A_{CS} = a \cdot b + \pi \left( \frac{b}{2} \right)^2, \quad (3.1)$$

where  $a$  is the height of the pipe, and  $b$  is the width of the pipe. The wetted perimeter is calculated as

$$L_{WP} = 2a + \pi b. \quad (3.2)$$

The hydraulic diameter is calculated as

$$D_H = 4 \frac{A_{CS}}{L_{WP}}. \quad (3.3)$$

The layout of the coolant loop is presented in Fig. 3.1a. Each column of the pipe is modelled using three consecutive connected objects and each bend is modelled with one object. This sums up to 31 objects.

The total length of coolant loop for the whole battery pack is assumed to be 80 m, and splitted up to equal portions in the pipe-objects, except for the bends. The radius of the bend (from the center of the bend to the center of the pipe) is calculated as

$$R_b = 1.2b, \quad (3.4)$$

with the factor 1.2 arbitrarily chosen, and the length of each bend is

$$L_b = \pi R_b. \quad (3.5)$$

### 3.3.5 Flow Boundary (*EndEnvironment*)

The *EndEnvironment* object is used to set inlet and outlet boundary conditions pressure, temperature, and fluid composition.

### 3.3.6 Solid Walls (*ThermalMass*)

The *ThermalMass* is defined as one-dimensional objects with two surfaces (called "ports"). The ports' emissivity (set to zero), distance to the center, and area is set. For the whole object, its mass, initial temperature, and material is specified (for more detail, see section 3.2).

In this system the object is used to model the pipe walls and the battery module-walls, the latter being composed of 41 objects in total. The pipe wall is splitted into two (one side facing the module wall and one facing the lumped battery cells) meaning the area of the *ThermalMass* modelling each part is half of the total surface area. Further, the pipe is splitted perpendicular to the flow, placing a separate pipe wall next to each lumped group of battery cells.

The area per battery module-wall section above and below the lumped battery cells are calculated as

$$A_{roof} + A_{floor} = 2(R_b - 0.5b - r)L. \quad (3.6)$$

The *ThermalMasses* representing adjacent pipe wall-object (those on each side of a section of the flow, or those next to each other placed along the flow, see Fig. 3.2) or module wall-parts that in reality are connected and able to conduct heat to each other are not connected with *ConductanceConn* in this model, i.e. the conductance between the adjacent parts is neglected.

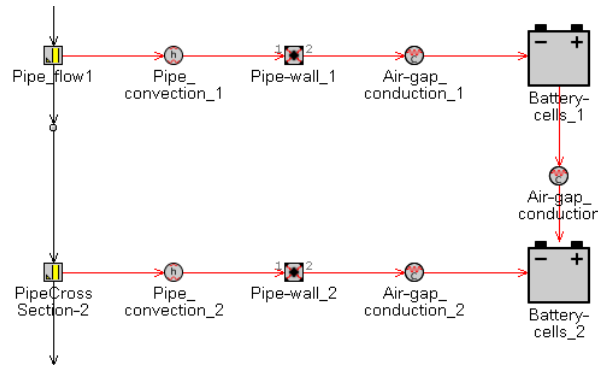


**Figure 3.2:** Section of the model. "Pipe-wall\_1" and "Pipe-wall\_2" are representing parts of the coolant pipe which are in reality connected to each other as one part.

### 3.3.7 Battery Cells (*ThermalBlock*)

The *ThermalBlock* models a rectangular cuboid with its three dimensions specified as  $L$ ,  $a + b$ , and  $2(R_b - 0.5b - r)$ . These are used to calculate its six surfaces (ports) connected to surrounding heat transfer objects. A source heat is user-defined as

$$Source\ Heat = (Power\ Request) \cdot (1 - Efficiency). \quad (3.7)$$

The material is specified as aluminum, with the dimensions of the block calculated from the dimensions of the pipe.

In this system *ThermalBlock* is used as one of two approaches to model a set of lumped battery cells. The advantage of this object compared with *Battery* is that its heat rate can be specified, and thus enabling of a higher thermal loss compared with only battery cells. This is done to try and include the heat generated from the electrical wires, even though this is poorly modelled and not correctly located.

### 3.3.8 Battery Cells (*Battery*)

Another object used to model the lumped battery cells is *Battery*, wherein the cells (due to lack of data) are only connected in series. The behaviour of this object is described in section 2.3. In addition, its specifications are the same as for *ThermalBlock* described in section 3.3.7. Data for the battery cells was retrieved from the article published by Hussein [36]. The battery capacity was 1.1 Ah, and  $V_{OC}$  and  $R_{int}$  are presented in Fig. 3.3 and Table 3.2.

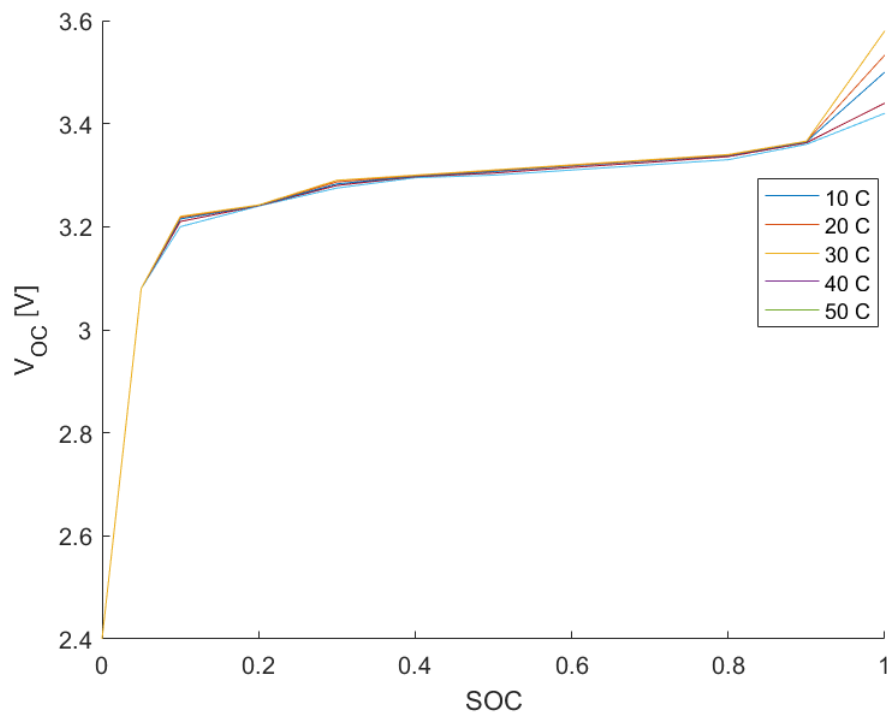


**Figure 3.3:** Open circuit voltage as a function of state of charge and temperature.

**Table 3.2:** Internal resistance for both 1E and E/2 as function of temperature

T [°C]	10	20	30	40	50
$R_{int}[\Omega]$	0.2	0.175	0.15	0.125	0.1

Two different constant battery power requests were investigated: one which depletes the battery after 1 hours and one which depletes it after 2 hours. These power requests were 252 W and 126 W per group of lumped battery cells, respectively.

These power requests were based on a Tesla S with a battery capacity of 85 kWh. The number of cells in each group is tuned to nearly fully deplete the lumped cells (circa 5 % of SOC left) after 2 hours at 126 W or 252 W power request, i.e. the power request is  $E/2$  and  $E$ , respectively.

#### 3.3.9 Controller (*PIDController*)

A PID-Controller is used to control the volumetric flow (the output) in the coolant loop by manipulating the pump speed (the input). The object *PIDController* is connected to the object of interest via a *SensorConn* object, and connected to the *SpeedBoundaryRot* (via a *ActuatorConn* object) which sets the pumping speed of the pump.

##### 3.3.9.1 Tuning the Controller

To tune the controller, a step response is produced to extract characteristics of the system. The step response is produced by initially keeping the input (the pump speed) at a constant until the output (the volumetric flow) is at a steady-state, then the input is changed over a time of 10  $\mu\text{s}$  and data is extracted as described in section 2.9.1 after a new steady-state has established.

#### 3.3.10 Temperature (*Temperature*)

The *Temperature* object is used to set a temperature used in the modelling of convective heat transfer from a *ThermalMass* object.

## 3.4 Modelling the Coolant Circuit

To model the flow of coolant through the circuit, the objects are connected in the following way: *EndEnvironment* (supplying the inlet conditions) to *PipeCrossSection* to *Pump* to a series of *PipeCrossSections* (some of which model bends of the pipe) to *EndEnvironment* (supplying the outlet conditions). The pump is controlled with the *PIDController* object which measures the flow in the *PipeCrossSection* out from the *Pump*. This system is depicted in Fig. 3.4, where "Pipe\_flow-2" substitutes a whole series of *PipeCrossSection* objects present in the actual model, the black arrows signify physical flow, and the blue arrows signify transfer of data.

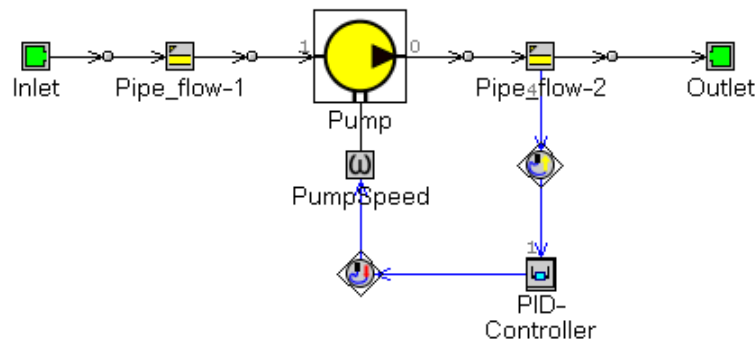


Figure 3.4: Modelling circuit of coolant.

## 3.5 Modelling Heat Transfer

To model the heat transfer, objects are connected to each other as follows.

### 3.5.1 Pipe to Battery Cells

Heat transfer from the pipe to the battery cells is modelled with objects connected in the following way: *PipeCrossSection* to *ConvectionConn* to *ThermalMass* to *ConductanceConn* to *Battery* or *ThermalBlock*, as depicted in Fig. 3.5. The red arrows signifies heat transfer.

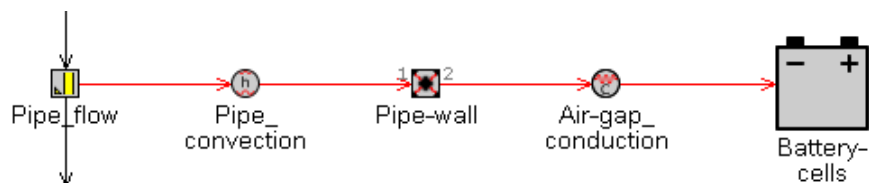


Figure 3.5: Modelling heat transfer the pipe to battery cells.

### 3.5.2 Pipe to Outside Module

Heat transfer from the pipe to the surrounding air outside the module walls is modelled with objects connected in the following way: *PipeCrossSection* to *ConvectionConn* to *ThermalMass* to *ConductanceConn* to *ThermalMass* to *ConvectionConn* to *Temperature*, as depicted in Fig. 3.6.

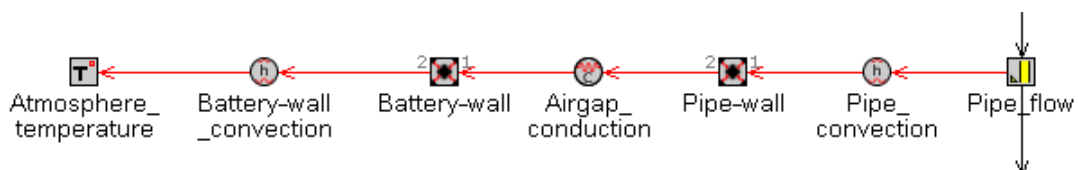


Figure 3.6: Modelling heat transfer from pipe to surrounding air outside module.

### 3.5.3 Battery Cells to Outside Module

Heat transfer from the battery cells to the surrounding air outside the module walls (both through the top, the bottom, and the side not covered by the pipe) is modelled with objects connected in the following way: *Battery* or *ThermalBlock* to *ConductanceConn* to *ThermalMass* to *ConvectionConn* to *Temperature*, as depicted in Fig. 3.7.



**Figure 3.7:** Modelling heat transfer from battery cells to the surrounding air outside the module.

### 3.5.4 Battery Cells to Battery Cells

Heat transfer between the lumped battery cells is modelled by connecting the adjacent *Battery* or *ThermalBlock* objects with a *ConductanceConn* object, as depicted in Fig. 3.8.



**Figure 3.8:** Modelling heat transfer between battery cells.

# 4

## Results and Discussion

### 4.1 Heat Production

The thermal loss of the battery cells are about 2.42 % of supplied electrical energy at a power request of 126 W (22.12 kJ in total for 2 hours, see Fig. 4.1) and 4.4 % at 252 W (39.91 kJ in total for 1 hour, see Fig. 4.2).

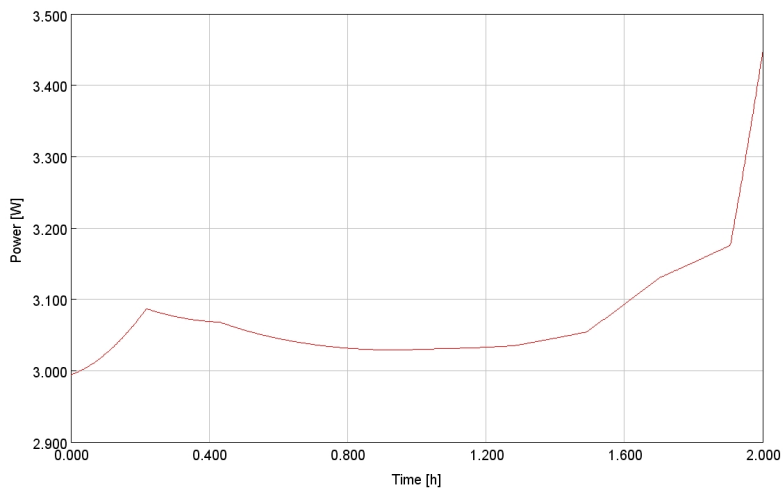


**Figure 4.1:** Heat dissipation of a group of lumped battery cells at  $E/2$ .

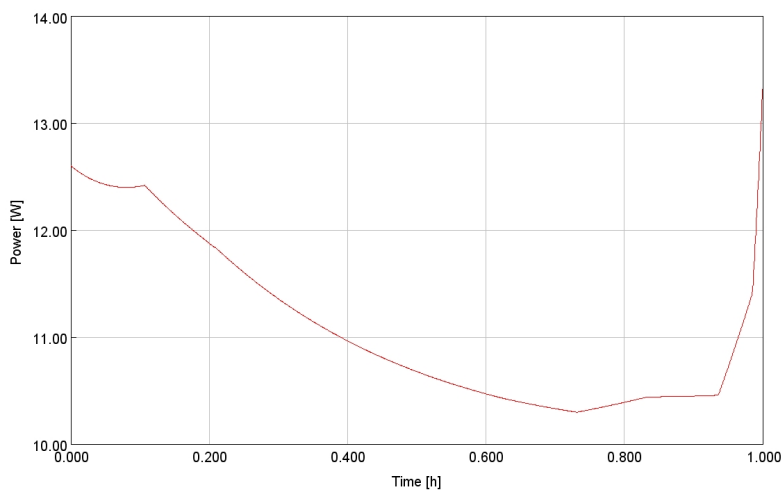


**Figure 4.2:** Heat dissipation of a group of lumped battery cells at  $1E$ .

At the end of each plot, the rate of heat dissipation increases sharply; this is due to the drop in open circuit voltage at low SOC which leads to an increase in the current and in turn to a decrease in voltage delivered from the cells. The decrease in voltage delivered is more severe than the decrease in open circuit voltage, and this increasing difference between the two quantities and the increasing current both increase the heat dissipation rate of the battery cells. This is also the reason for the initial increase in the heat dissipation rate, since there is a drop in open circuit voltage between SOC of 1 to 0.9. Between these two points, the heat dissipation gradually decreases; this is due to the decreasing internal resistance which is a consequence of the increasing cell temperature.

### 4.2 Cell Temperature

The temperature of the cells at the two E-rates without active cooling can be seen in Fig. 4.3 and 4.4. It is worth pointing out that the coolant pipe is still filled with coolant, which helps to keep the battery cells cool.

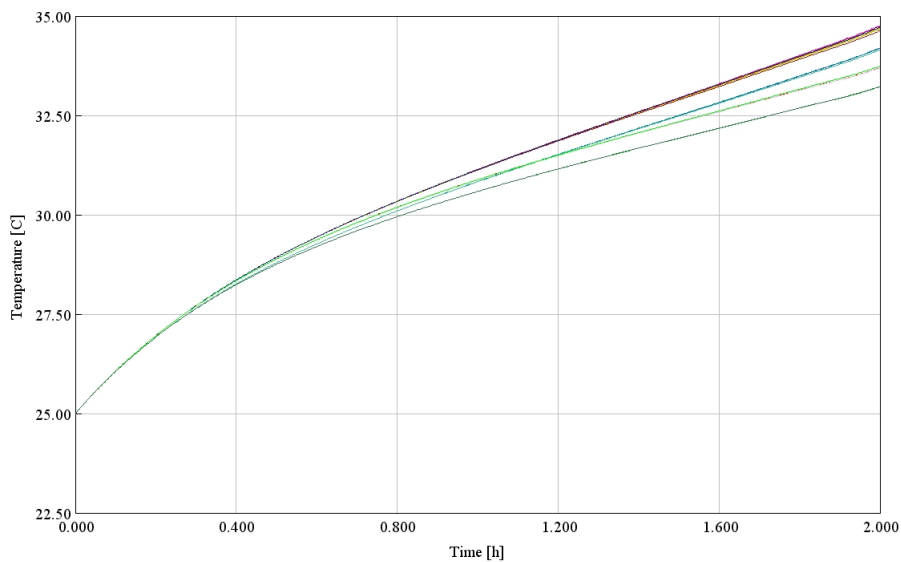


**Figure 4.3:** Temperature of lumped battery cells at power request of  $E/2$  without active cooling.

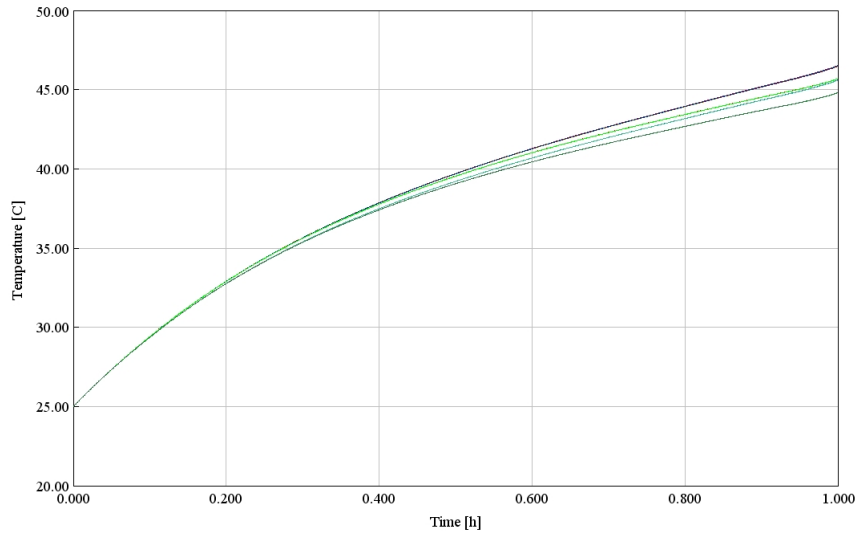


**Figure 4.4:** Temperature of lumped battery cells at power request of 1E without active cooling.

Each line represents the temperature of one group of lumped cells. Some of the lumped cell-group temperatures overlap, resulting in graphs which seems to include fewer lines than the number of groups of lumped cells. With an active cooling, the temperatures are decreased and the temperatures of the lumped cells deviated more from each other. The temperatures of the cells for different cooling rates (i.e. volumetric coolant flow rate per module) and E-rates can be seen in Fig. 4.5-4.10.

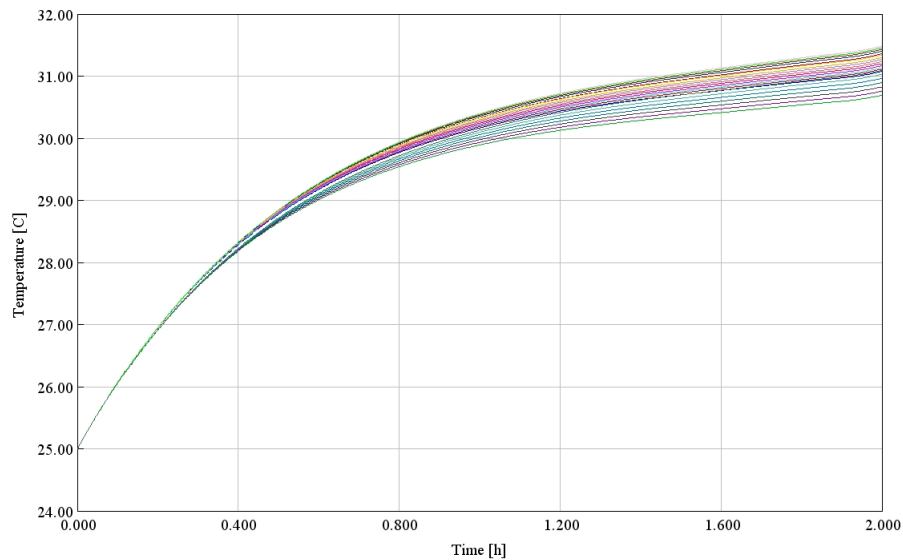


**Figure 4.5:** Temperature of lumped battery cells at power request of E/2 with cooling rate of 0.03 L/s.

Further increasing the volumetric coolant flow rate leads to the temperatures forming two clusters of temperatures, and the spread within these clusters become more narrow as the flow rate is increased. The lower set of data-points are those of the

## 4. Results and Discussion

---

lumped cells next to the bent pipe, seen in Fig. 3.1a and separated from the other cells by the gray dashed lines. This is since there will be a larger area of battery cells in contact with the coolant pipe, and the effects of this is more clearly seen at higher coolant flow rate.

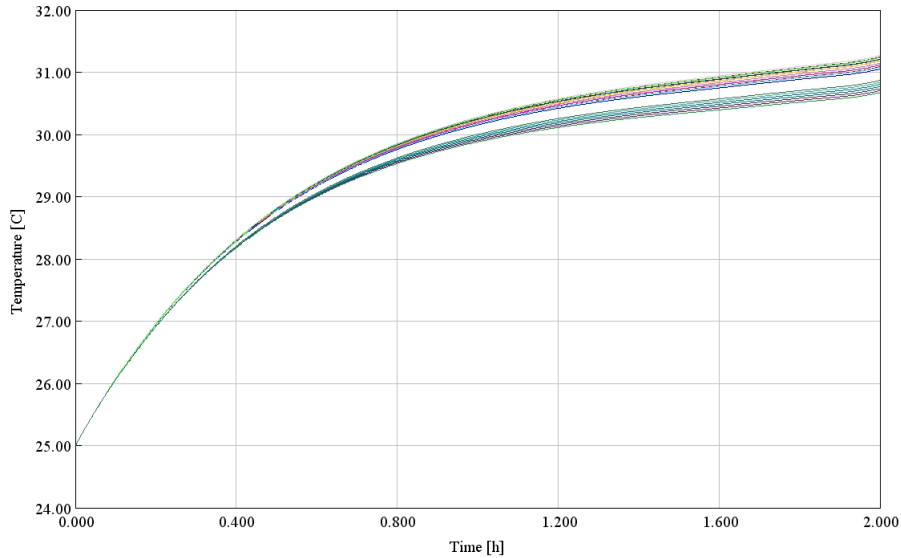


**Figure 4.6:** Temperature of lumped battery cells at power request of  $E/2$  and cooling rate of  $0.0625$  L/s.

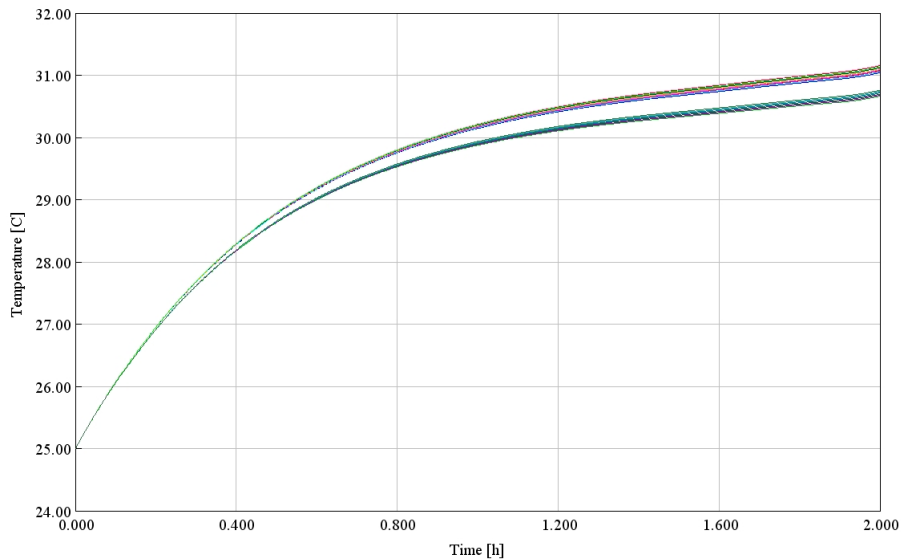


**Figure 4.7:** Temperature of lumped battery cells at power request of  $E/2$  and cooling rate of  $0.125$  L/s.

Increasing the E-rate to  $1E$  results in the cells becoming overheated. This is not solved by increasing the flow rate. In several of the simulations, towards the end of the simulation time when more steady conditions are reached, the temperature starts to increase more sharply. This is due to the increase in heat dissipation rate,

explained in section 4.1.

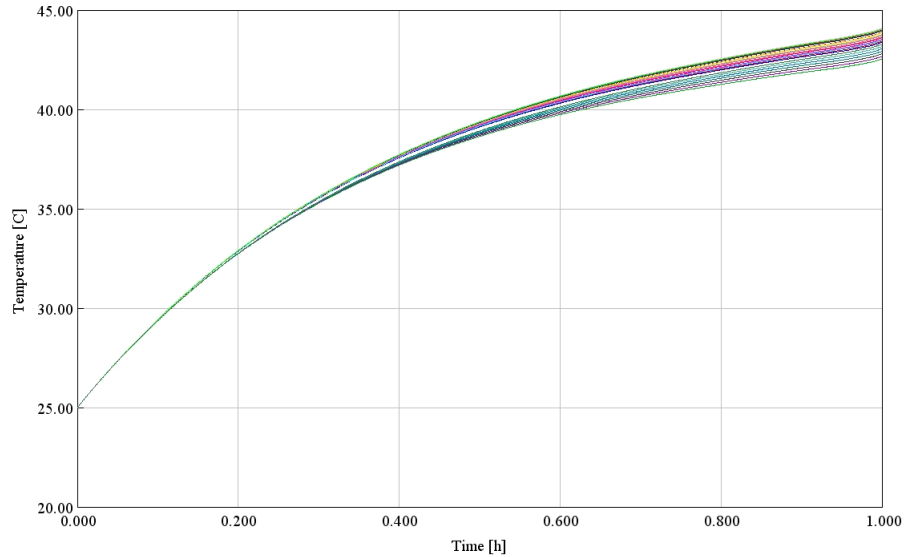


**Figure 4.8:** Temperature of lumped battery cells at power request of 1E and cooling rate of 0.03 L/s.

Similar trend of forming two clusters of temperatures is observed. This is consistent with the results at lower power request. However, the final temperatures of the battery cell groups are higher at 1E, which is expected.

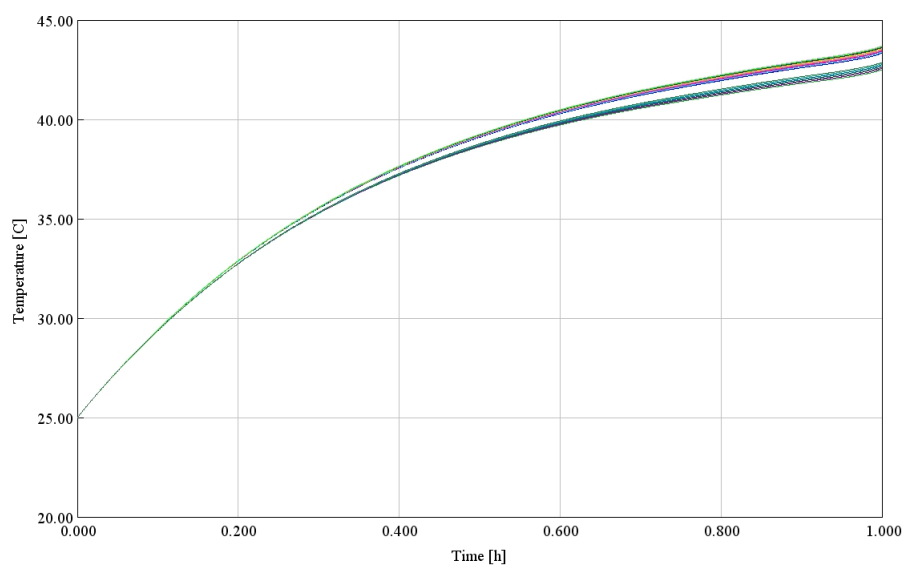


**Figure 4.9:** Temperature of lumped battery cells at power request of 1E and cooling rate of 0.0625 L/s.

## 4. Results and Discussion

---

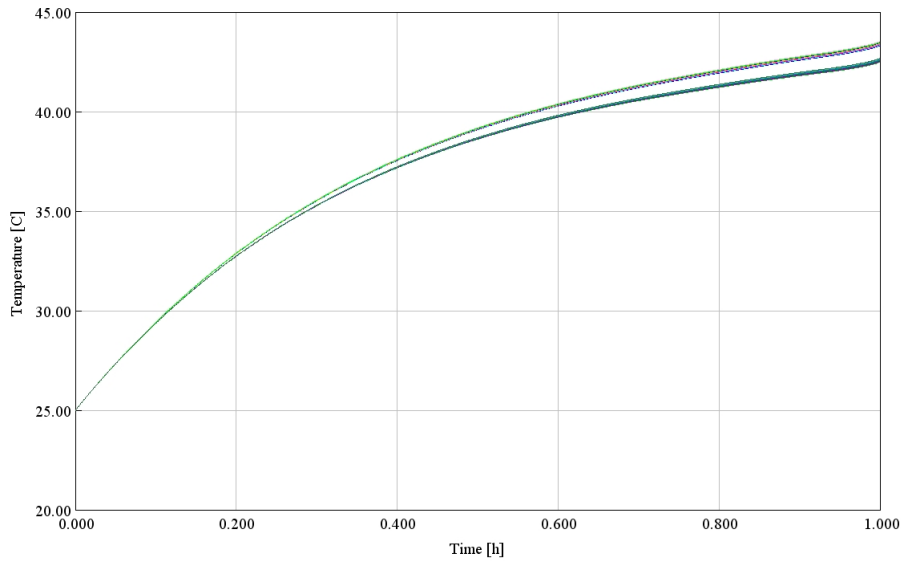


**Figure 4.10:** Temperature of lumped battery cells at power request of  $1E$  and cooling rate of  $0.125$  L/s.

Using *ThermalBlock* as a substitute for *Battery*-objects with these rates of heat production gave temperature plots that were in accordance with the results of using *Battery*-object. *ThermalBlock* was subsequently used to try and capture the effects of heat dissipation in the electrical wires in the battery. This was done by increasing the thermal loss twofold, and some of the results can be seen in Fig. 4.11 and 4.12

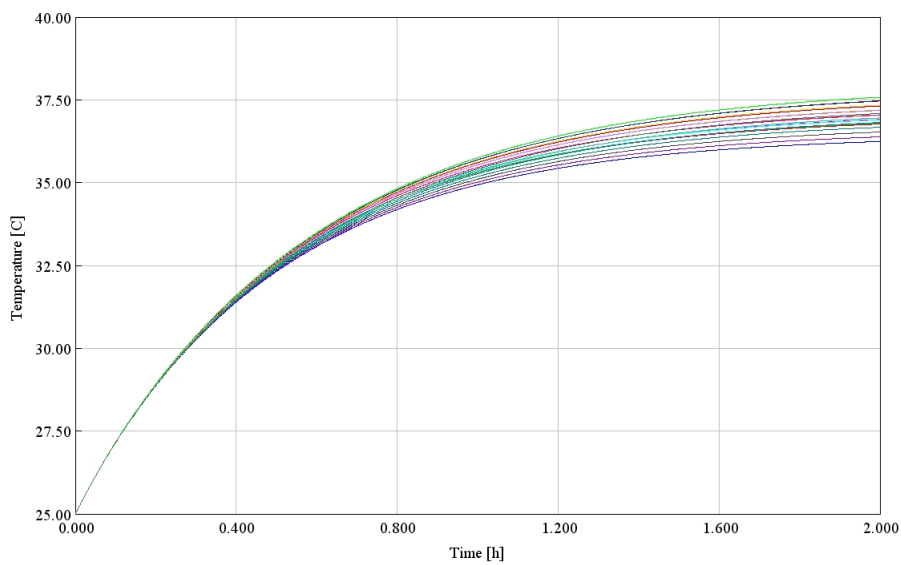


**Figure 4.11:** Temperature of lumped battery cells with approximately twice the heat dissipation of a battery at power request of  $E/2$  with cooling rate of  $0.03$  L/s

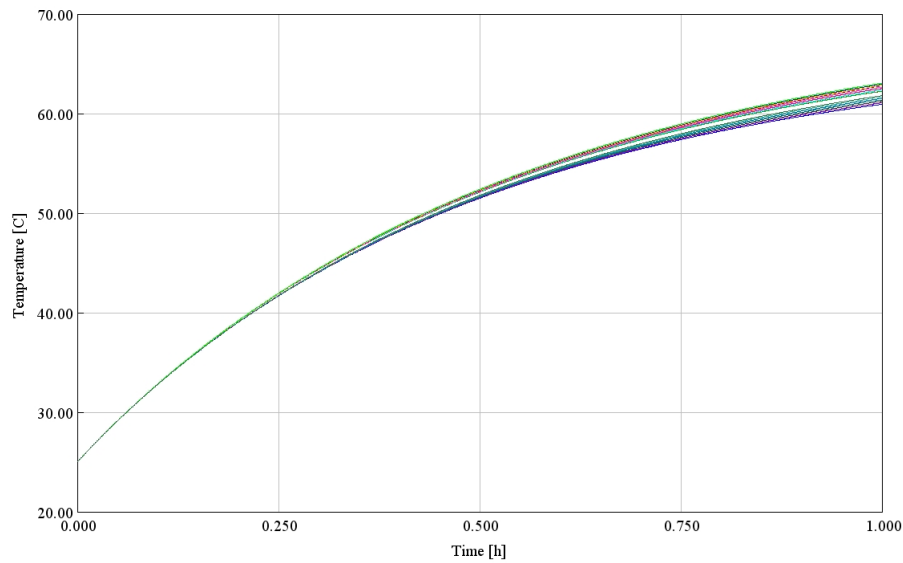


**Figure 4.12:** Temperature of lumped battery cells with approximately twice the heat dissipation of a battery at power request of 1E with cooling rate of 0.0625 L/s.

For more results, see Appendix A.

## 4.3 Heat Transfer

The interior convective heat transfer coefficient of the coolant pipe,  $h$ , is circa 40 W/m<sup>2</sup>K for all of the cases (even for stagnant coolant) since the flow remains laminar in all the simulations. The thermal resistance in the air-gap between the pipe and the batteries is 2.99 K/W and is the largest of the system. The resistance present at the inside of the coolant pipe is 1.03 K/W.

### 4.3.1 Assumptions

The assumption of constant wall temperature was investigated. In the majority of the system, the temperature difference between the adjacent *ThermalMass*-objects (see Fig. 3.2) was at most about 1-2 % (on a °C basis) and the assumption of negligible conductance is plausible. In the extreme cases, the temperature difference between adjacent pipe wall-objects was as large as 30 % and the assumption of no heat conduction is incorrect. This is only true for in the objects part of the pipe adjacent to the module wall. On the whole, this heat transfer is negligibly small in comparison with the total heat transfer of the system which makes it of no concern. This was also explicitly tested by including the conduction between the pipe wall-objects in simulations and its effects were deemed negligible. In addition, the large temperature difference between the pipe wall objects adjacent to the module wall and the objects of the other side of the pipe wall stems from the simplified boundary conditions of a constant uniform temperature surrounding the module.

Another assumption made was that of uniform temperature inside each battery cell (i.e. negligible internal thermal resistance). At the standard conditions investigated in the study,  $Bi$  is about 0.012. Thus, the assumption of negligible internal resistance of the battery cells is valid. The criterion of  $Bi = 0.1$  (used to decide if the internal resistance is negligibly small) is reached when the surrounding heat transfer coefficient reaches  $127 \text{ W}/(\text{m}^2 \cdot \text{K})$  [29].

### 4.3.2 Sensitivity Analysis and Heat Transfer Optimization

Increasing the coolant flow rate improves the cooling, not due to an increased convective heat transfer coefficient which basically stays the same, but due to the coolant keeping a lower temperature throughout the coolant pipe. The effects of increased coolant flow diminishes fast since the the coolant temperature in the whole pipe approaches the inlet temperature fast (already at 0.03 L/s the outlet temperature is  $26.7 \text{ }^\circ\text{C}$ ). To further increase the heat transfer, a Reynolds number above 2000 has to be reached which is achieved at 0.42 L/s. This is equivalent to a total flow of 6.72 L/s for the battery pack which is unfeasible. Adding roughness to the pipe does not either have an effect on the heat transfer since the flow is laminar. Solution which can not be implemented in the software but in reality is adding dimples inside the pipe to induce turbulence or fins to increase the heat transfer area. Another improvement for real batteries which Tesla S implements in the 100 kWh batteries is using two consecutive coolant pipes per module [24]. In these simulations, this change would have no large effect since the problem is not to keep the coolant temperature cool but to increase the heat transfer coefficient.

In the present model, the largest thermal resistance is present in the small air-gap between the coolant pipe wall and the battery cells where conduction is taking place. To affect the resistance of the convection of the coolant flow, the effects of changing the dimensions of the pipe was investigated. Increasing the length of the pipe twofold decreases both the convection and conduction resistance by half, while decreasing the air-gap between the pipe wall and battery cells to half its size decreases only the conductance resistance by half. Though the change in the dimensions are relatively the same, it needs to be kept in mind that the former change represents a total increase of about 5 m of pipe per module, while the latter is only a question of how tight the pipe wall is placed against the cells. Its effects can be seen in Fig. 4.13 and 4.14.

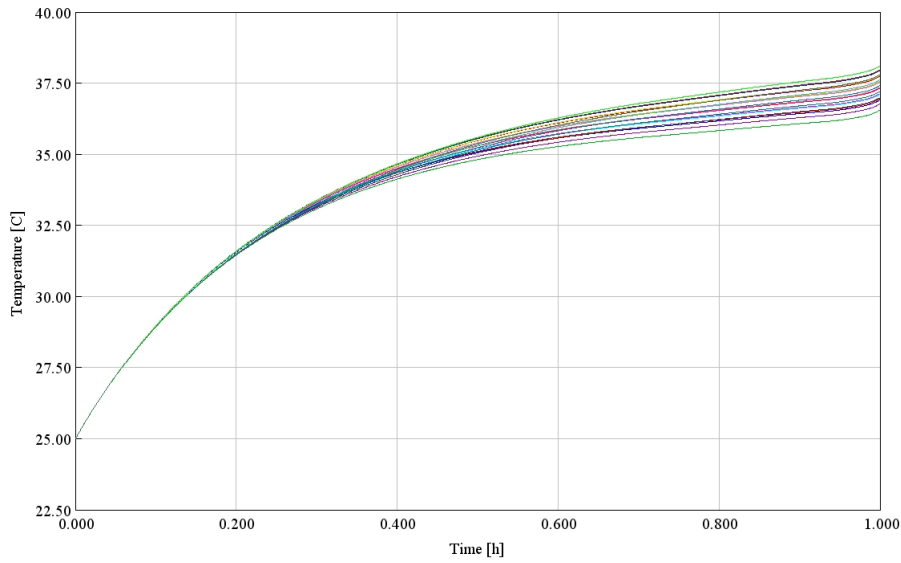


**Figure 4.13:** Temperature of lumped battery cells with cooling rate of 0.03 L/s, power request of 1E, and the length per pipe-object is multiplied by 2.

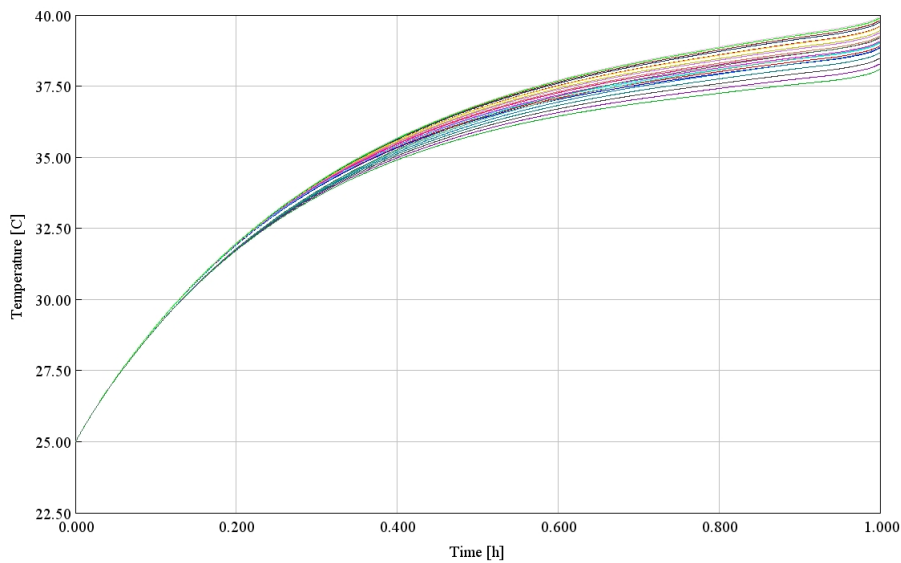


**Figure 4.14:** Temperature of lumped battery cells with cooling rate of 0.03 L/s, power request of 1E, and air-gap halved to 0.8 mm.

Under these conditions, it's crucial that the properties of the air-gap is correctly specified if they are to give accurate simulations of a real system. Another way of modelling the air-gap would be with convection. To increase the heat transport between the coolant pipe and the battery cells further, the gap could be filled with highly conducting material (such as thermal paste) but this was not further investigated in the study due to time limitations. This is probably customary in the industry already, but due to lack of data this could not be confirmed. Exterior convective cooling was of negligible influence. Simulations with no heat transfer at the module walls resulted in cell temperatures changing less than 1 % compared

with the those where exterior heat transfer was present. Spatial resolution was of negligible influence. Increasing the time step lead to the pump taking longer time to reach steady state due to instabilities, and at a large enough time step (at circa 1.5 s) it was unable to reach steady state. Up til this point the different time steps did not affect the simulation results.

## 4.4 Controller

The *PIDController* was tuned for 0.125 L/s, but worked well for a wide range of flows. The extracted data from the step response can be seen in Table 4.1.

**Table 4.1:** Data extracted from step response.

Slope [L/(s·RPM)]	Time Constant [s]	Settling Time [s]
$6.69 \cdot 10^{-4}$	3	10

## 4.5 System Data

To further validate the model, real data for a battery system needs to be used. The battery capacity which is supposed to be that of a real Tesla Model S may not be correct either. It's up for debate how much actual capacity the battery has, for example it is discussed in an article in Electrek [32]. Since the aim of the project was not to model a Tesla S, but to develop a generic model of an electric car module, it was of no concern but something to keep in mind when using data to validate the model.

# 5

## Conclusions and Future Work

The model was able to complete simulations of nearly full discharge of a battery module under one minute, incorporating the phenomena important for the thermal management of the cells. The simulation was robust to changes in both spatial and temporal discretization. In the former case there were no significant effects on the results and the maximum size was only limited by the size of the system and the latter being limited by instabilities in the controller of the pump. The assumptions of uniform pipe wall temperature and negligible internal thermal resistance in the battery cells were both deemed suitable.

The external cooling was of minor importance in the model. The largest thermal resistance was present in the space between the pipe and the battery cells. The battery cell temperatures were highly sensitive to the width of this space, and a simple solution to decrease the resistance, besides narrowing the gap, would be to have this space occupied by a material with high thermal conductivity. It is likely that this is applied in actual electric car batteries already, but due to lack of data this could not be confirmed. The model should be suitable for conceptual studies or early-stage modelling after further improvements have been implemented.

To validate the model, real battery data needs to be used. Sources of heat production that in all probability needs to be included are the ones taking place in the electric circuits, and future models should thus implement this. To possibly get a higher level of detail, implementation of equations for battery chemistry can be considered. The model can be expanded to include the whole battery pack, not just one module. This will probably enable the use of more suitable boundary conditions at the walls. Further more, for batteries with even higher capacity, two coolant pipes per module, as in the new 100 kWh Tesla batteries, can be investigated [24]. Under certain climates, *heating* of the battery cells can be relevant, which could be of interest to investigate. If this is investigated, the battery capacity's dependency on temperature should probably be implemented.



# Bibliography

- [1] D. Sperling and D. Gordon, *Two Billion Cars: Driving Toward Sustainability*. Oxford University Press, 2009.
- [2] A. F. D. Center. Fuel properties comparison. [Online]. Available: [http://www.afdc.energy.gov/fuels/fuel\\_comparison\\_chart.pdf](http://www.afdc.energy.gov/fuels/fuel_comparison_chart.pdf)
- [3] K. E. Aifantis, S. A. Hackney, and R. V. Kumar, *High Energy Density Lithium Batteries: Materials, Engineering, Applications*. Wiley-VHC, 2010.
- [4] A. Yoshino. Course of development of the lithium-ion battery, and future outlook. [Online]. Available: <https://www.natureasia.com/en/advertising/PDF/tech-forum/01/Asahi-Kasei.pdf>,
- [5] D. Bernadi, E. Pawlikowski, and J. Newman, “A general energy balance for battery systems,” *Journal of the Electrochemical Society*, vol. 132, no. 1, pp. 5–12, May 1984.
- [6] A. M. P. Brookes, *Basic Electric Circuits (Second Edition)*, 2nd ed., August 1975.
- [7] L. Lua, X. Hana, J. Lia, J. Huab, and M. Ouyanga, “A review on the key issues for lithium-ion battery management in electric vehicles,” *Journal of Power Sources*, vol. 226, March 2011.
- [8] Z. Rao and S. Wang, “A review of power battery thermal energy management,” *Renewable and Sustainable Energy Reviews*, vol. 15, no. 9, December 2011.
- [9] A. A. Pesaran, A. Vlahinos, and S. D. Burch, “Fourteenth international electric vehicle symposium,” in *Thermal Performance of EV and HEV Battery Modules and Packs*, Florida, September 1997.
- [10] A. A. Pesaran, “Advanced automotive battery conference,” in *Battery Thermal Management in EVs and HEVs: Issues and Solutions*, Nevada, February 2001.
- [11] M. Doyle, T. F. Fuller, and J. Newman, “Modeling of galvanostatic charge and discharge of the lithium/polymer/insertion cell,” *Journal of Electrochemical Society*, vol. 140, no. 6, pp. 1526–1533, 1993.
- [12] P. M. Gomadam, J. W. Weidner, R. A. Dougal, and R. E. White, “Mathematical modeling of lithium-ion and nickel battery systems,” *Journal of Power Sources*, vol. 110, no. 2, pp. 267–284, 2002.
- [13] X. Hua, S. Lia, and H. Penga, “A comparative study of equivalent circuit models for li-ion batteries,” *Journal of Power Sources*, vol. 198, pp. 359–367, 2012.
- [14] L.-R. Dung, H.-F. Yuan, J.-H. Yen, C.-H. She, and M.-H. Lee, “A lithium-ion battery simulator based on a diffusion and switching overpotential hybrid model for dynamic discharging behavior and runtime predictions,” *Energies*, vol. 9, no. 1, 2016.

- [15] K. W. Choi and N. P. Yao, “Heat transfer in lead-acid batteries designed for electric vehicle propulsion application,” *Journal of Electrochemical Society*, vol. 126, no. 8, pp. 1321–1328, 1979.
- [16] T. M. Bandhauer and S. Garimella, “Passive, internal thermal management system for batteries using microscale liquid–vapor phase change,” *Applied Thermal Engineering*, vol. 61, no. 2, pp. 756–769, 2013.
- [17] P. Atkins, L. Jones, and L. Laverman, *Chemical Principles*, 7th ed. W. H. Freeman Co Ltd, 2016.
- [18] *Lithium Ion technical handbook*, Gold Peak Industries Ltd., 2003.
- [19] *GT-Suite Flow Theory Manual*, Gamma Technologies, 2016.
- [20] *A Guide to Understanding Battery Specifications*, MIT Electric Vehicle Team, 2008.
- [21] B. Hoerman, “Phev, hev, and ev battery pack testing in a manufacturing environment,” <https://www.dmcinfo.com/latest-thinking/white-papers/id/151/phev-hev-and-ev-battery-pack-testing-in-a-manufacturing-environment>, Tech. Rep.
- [22] E. Musk. (2013) Model S Fire. [Online]. Available: [https://www.tesla.com/sv\\_SE/blog/model-s-fire?redirect=no](https://www.tesla.com/sv_SE/blog/model-s-fire?redirect=no)
- [23] D. Biello. (2013) How tesla motors builds one of the world’s safest cars [video]. [Online]. Available: <https://www.scientificamerican.com/article/how-tesla-motors-builds-the-safest-car-video/>
- [24] F. Lambert. (2017) Teardown of new 100 kwh tesla battery pack reveals new cooling system and 102 kwh capacity. [Online]. Available: <https://electrek.co/2017/01/24/tesla-teardown-100-kwh-battery-pack/>
- [25] U. M. Ascher, S. J. Ruuth, and R. J. Spiteri, “Implicit-explicit runge-kutta methods for time-dependent partial differential equations,” *Applied Numerical Mathematics*, vol. 25, no. 2-3, 1997.
- [26] R. Courant, K. Friedrich, and H. Lewy, “Über die partiellen differenzgleichungen der mathematischen physik,” *Mathematische Annalen*, vol. 100, no. 1, pp. 32–74, 1928.
- [27] T. L. Bergman, A. S. Lavine, F. P. Incropera, and D. P. DeWitt, *Fundamentals of Heat and Mass Transfer*, 6th ed. USA: John Wiley Sons, 2006.
- [28] W. M. Kays and M. E. Crawford, *Convection Heat and Mass Transfer*, 3rd ed. New York: McGraw-Hill, 1993.
- [29] J. R. Welty, G. L. Rorrer, R. E. Wilson, and C. E. Wicks, *Fundamentals of Momentum, Heat and Mass Transfer*, 5th ed. John Wiley Sons, 2007.
- [30] T. Glad and L. Ljung, *Reglerteknik*, 4th ed. Studentlitteratur AB, 2006.
- [31] G. Bower, “Tesla or gm: Who has the best battery thermal management?” 2016. [Online]. Available: <http://insideevs.com/tesla-or-gm-who-has-the-best-battery-thermal-management-bower/>
- [32] F. Lambert. (2016) Tear down of 85 kwh tesla battery pack shows it could actually only be a 81 kwh pack. [Online]. Available: <https://electrek.co/2016/02/03/tesla-battery-tear-down-85-kwh/>
- [33] American Society of Heating, Refrigerating and Air-Conditioning Engineers, *ASHRAE Fundamentals Handbook*, Atlanta, June 1997.

- [34] J. Mattingly and H. von Ohain, *Elements of Propulsion: Gas Turbines and Rockets*. Reston, VA: American Institute of Aeronautics and Astronautics, Inc, 2006.
- [35] Teslarati Network. (2013) Tesla model s weight distribution. [Online]. Available: <https://www.teslarati.com/tesla-model-s-weight/>
- [36] A. A. Hussein, "Applied power electronics conference," in *Experimental Modelling and Analysis of Lithium-ion Battery Temperature Dependence*, North Carolina, March 2015.



# A

## Appendix

Additional simulation results of lumped battery cell temperatures for varying coolant flow rate and power request.

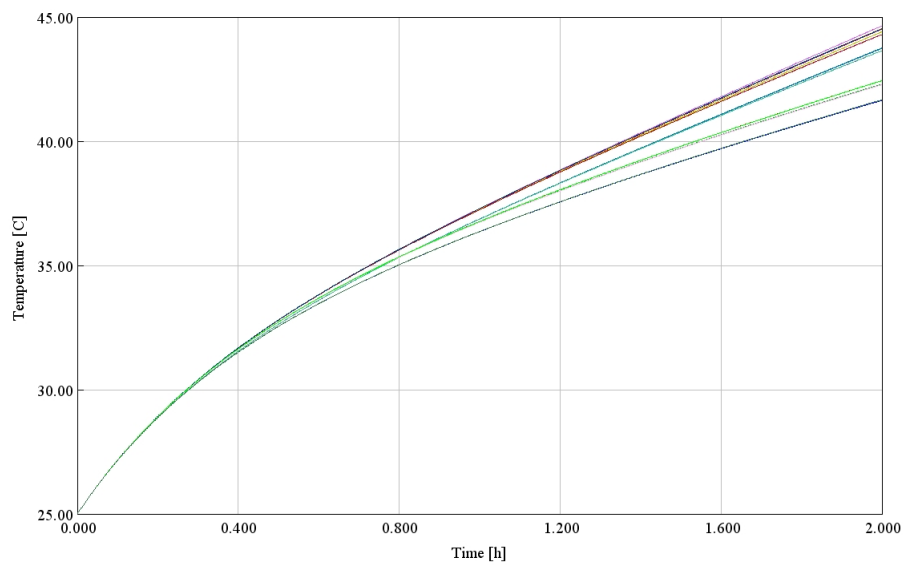


**Figure A.1:** Temperature of lumped battery cells with approximately twice the heat dissipation of a battery at power request of  $E/2$  without active cooling.

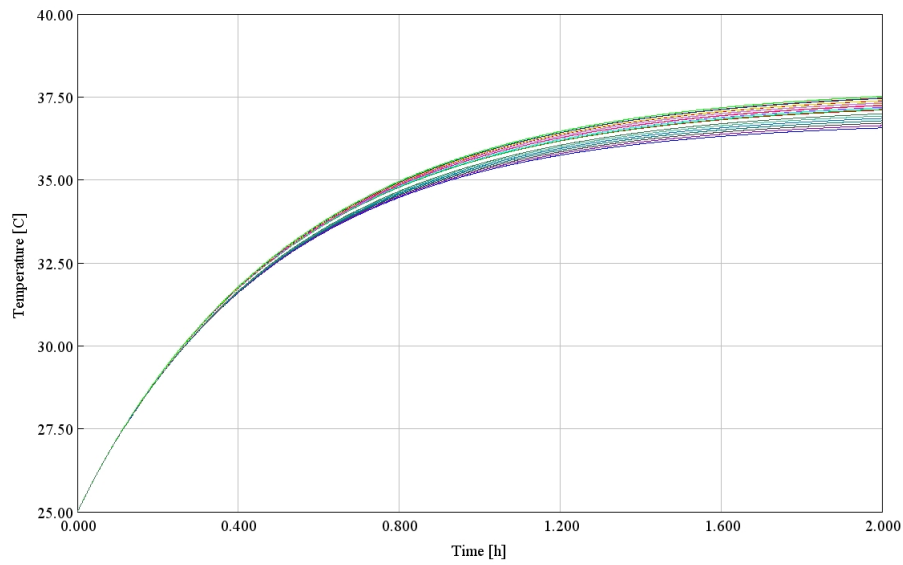


**Figure A.2:** Temperature of lumped battery cells with approximately twice the heat dissipation of a battery at power request of  $E/2$  with cooling rate of 0.0625 L/s.

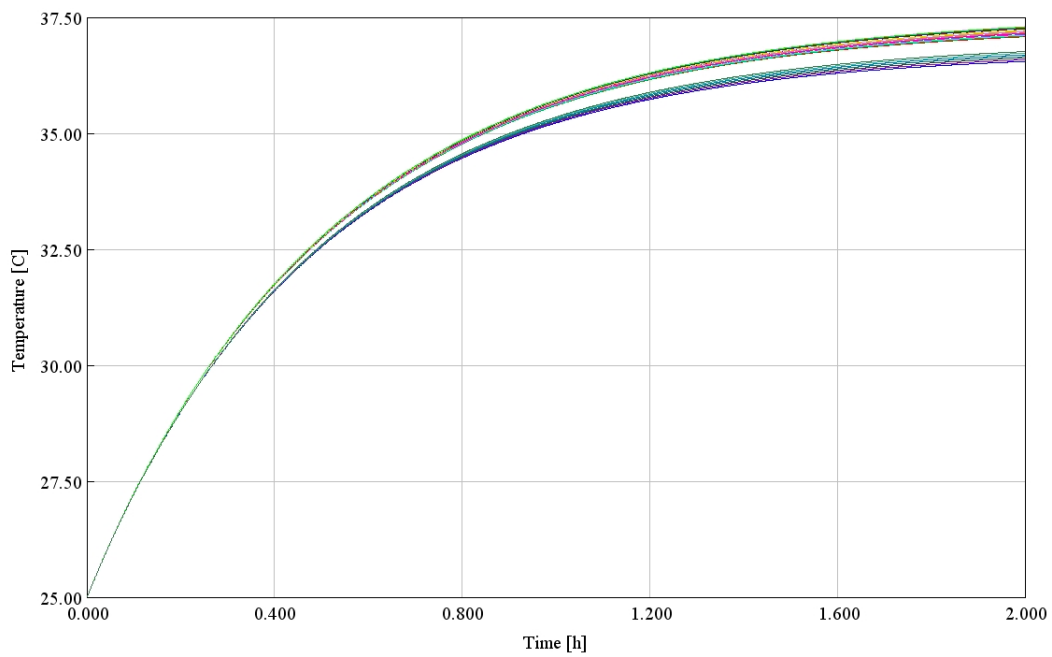


**Figure A.3:** Temperature of lumped battery cells with approximately twice heat dissipation of battery cells at  $E/2$  with cooling rate of 0.125 L/s.

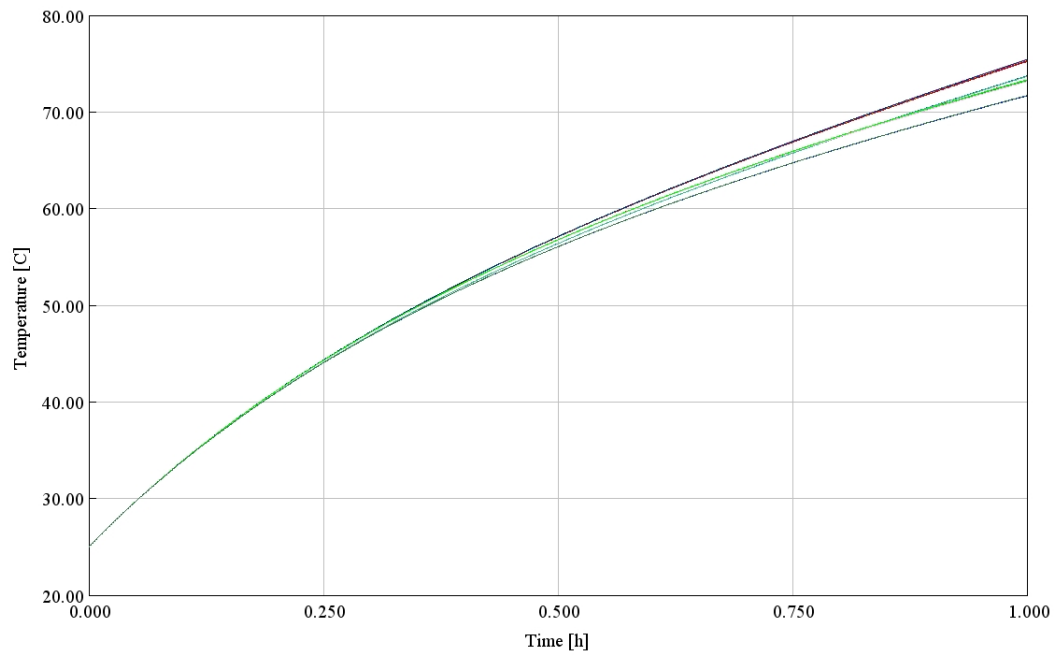


**Figure A.4:** Temperature of lumped battery cells with approximately twice the heat dissipation at 1E without active cooling.

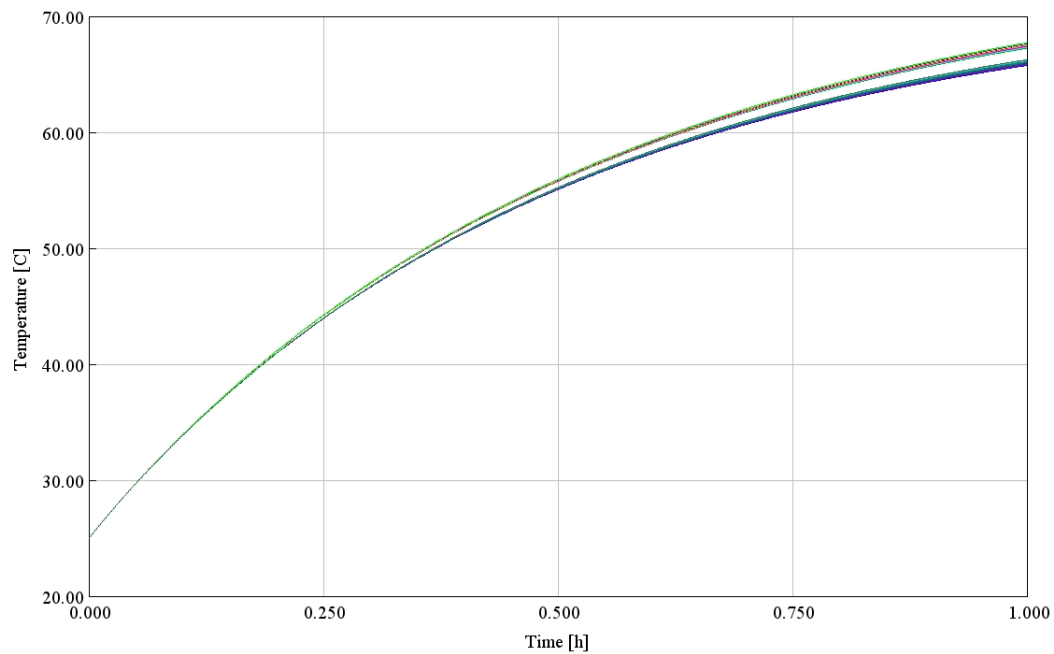


**Figure A.5:** Temperature of lumped battery cells with approximately twice the heat dissipation at 1E with cooling rate of 0.125 L/s.